J. Fluid Mech. (1986), *vol.* 162, *pp.* 463–487
Printed in Great Britain

Circulation measurements and vortical structure in an inlet-vortex flow field

By H. W. SHIN†, E. M. GREITZER†, W. K. CHENG‡, C. S. TAN† AND C. L. SHIPPEE‡
Massachusetts Institute of Technology, Cambridge, MA 02139

(Received 28 February 1985 and in revised form 30 July 1985)

An investigation has been conducted of the three-dimensional flow associated with the inlet-vortex phenomenon. Quantitative measurements were made of inlet- and trailing-vortex circulation and position. Flow visualization was used to obtain information on the overall structure of the vorticity field. It is shown that the inlet vortex and the trailing vortex have essentially equal and opposite circulation. In addition, the production of vorticity, due to vortex stretching, is the mechanism by which both of these are maintained. A limited parametric study was also conducted to define the circulation and position (in the inlet) of the inlet vortex, for parameters of practical engineering interest.

1. Introduction

Gas-turbine engine operation near the ground is often associated with the presence of a strong vortex which stretches between the ground and the engine inlet. This 'inlet vortex' (or ground vortex, as it is sometimes called) can be of concern because of the effects it can have on the engine; these include foreign-object damage, increased blade erosion due to dirt ingestion (Younghans & Paul 1978), and compressor surge (Motycka 1976).

Investigations of the inlet vortex have identified two basic mechanisms responsible for its formation (De Siervi *et al.* 1982, which we will refer to as DS). The first is the amplification of the *vertical* component of existing ambient vorticity as the vortex lines are convected into the inlet. A detailed description of this process, including calculations of the drift of these vertical vortex lines in the three-dimensional flow produced by an inlet near a ground plane, is given in DS.

The second mechanism for vortex formation, however, does *not* depend on the presence of ambient vorticity, and, for an inlet in cross-wind, can occur in a flow that is irrotational far upstream. In this situation, there is a variation in circulation along the inlet, and hence a trailing vortex (from the rear side of the inlet) also. It is this second mechanism, which is much less understood, that is discussed in the present paper.

2. Background

The principal kinematic parameters pertinent to the flow regimes encountered with an inlet/ground-plane configuration are the inlet average velocity U_i, the far

† Department of Aeronautics and Astronautics.
‡ Department of Mechanical Engineering.

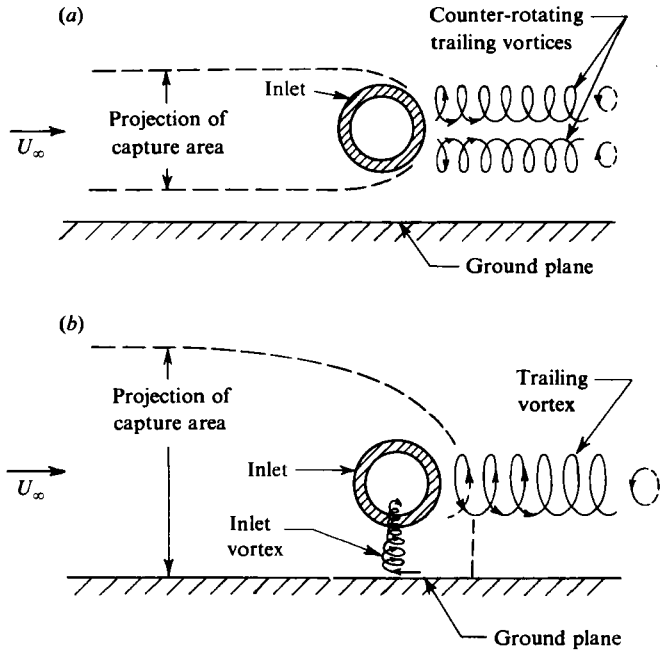

FIGURE 1. Flow regimes (inlet in cross-wind) (*a*). Low *CR*. (*b*) High *CR*.

upstream velocity U_∞, the inlet outside and inside diameters D and D_i, the inlet yaw angle α, and the height of the inlet centreline above the ground plane H. Other parameters associated with the specific geometry of the inlet might be introduced as well, although for the present study the above-mentioned set is sufficient.

For a given angle of yaw, α, the remaining dimensional quantities may be grouped into three non-dimensional parameters: the 'capture ratio' CR defined as $U_i D_i^2/U_\infty D^2$, the height-to-diameter ratio H/D, and the diameter ratio D_i/D. Although other equivalent groupings can be made, this one is used because, for a given CR and H/D, changes in the inlet geometry as reflected in the diameter ratio should not strongly influence the overall features of the flow. A description of the flow regimes using the two parameters CR and H/D should thus have a wider generality than one using the variables U_i/U_∞ and H/D_i, as is customarily done. We shall therefore use the former two parameters as the ones that have the most significant effects on the flow field.

At low values of capture ratio, and/or high values of H/D, an inlet in cross-wind in an upstream irrotational flow will have two counter-rotating vortices trailing from the rear of the inlet. These are depicted in figure 1(*a*), which is taken from the hydrogen-bubble flow-visualization studies reported previously (DS). Increasing the capture ratio, or decreasing H/D, leads to the formation of an inlet-vortex/trailing-vortex system, as indicated in figure 1(*b*).

As described in DS, the presence of this trailing vortex is associated with a variation in circulation (i.e. circulation round the inlet) along the length of the inlet. A *schematic* of the location of the vortex lines in the flow of figure 1(*b*) is given in figure 2. The circulation around curve C_2, which is just forward of the inlet lip and encloses the inlet vortex, is Γ_2. Far from the lip, around curve C_1, the circulation is small because the velocities are much lower than at the lip and the flow is roughly symmetric about the upper and lower part of the cylinder. Since $\Gamma_1 \ll \Gamma_2$, there must therefore be a

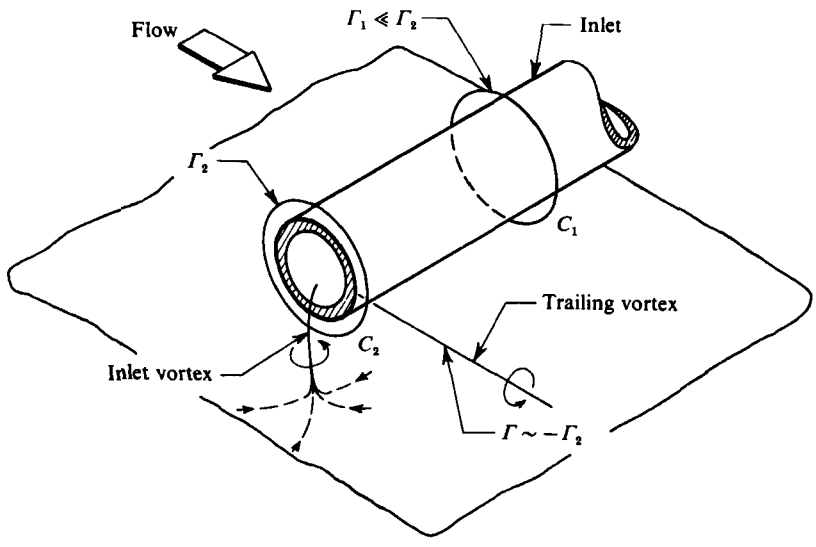

FIGURE 2. Inlet-/trailing-vortex system.

trailing vortex with circulation of strength approximately $-\Gamma_2$, as indicated in the figure.

The water-tunnel investigations of the inlet vortex, carried out previously, were only qualitative in nature. In particular, they provided only very rough estimates of the key fluid-mechanic parameters: vortex strength and position inside the inlet. These are required for the determination of the extent of non-uniformity (distortion) presented to the engine, as well as the degree to which particles will be ingested. The present study was thus undertaken to provide quantitative measurements of the three-dimensional vortex flow. As reported by Liu, Greitzer & Tan (1985), a facility for making these measurements was designed, built, and calibrated. Initial measurements in this facility showed that the overall structure of the flow field agreed with the conceptual picture developed from the water-tunnel observations.

The present paper presents the first detailed measurements of the three-dimensional flow associated with an inlet vortex. Several main points are addressed. In the order in which they are described below, the first is the quantitative demonstration that the circulation of the inlet and trailing vortices are (as hypothesized in DS) essentially equal and opposite. The second is the definition of inlet-vortex circulation and location (inside the inlet) for values of the relevant non-dimensional parameters representative of those occurring for actual aircraft, since this is a situation of strong practical interest. Third, new information about the vortical structure of these flows, which has been obtained from flow-visualization experiments in both water and wind tunnels, will be presented and discussed.

3. Experimental facility and experiment design

The measurements were conducted in the MIT Wright Brothers Wind Tunnel, a layout of which is shown in figure 3. The tunnel is closed-circuit, with an elliptical test section 3.05 m wide, 2.3 m high and 4.6 m long. During this investigation, a ground plane (with leading edge rounded and drooped to avoid flow separation) was mounted 0.5 m above the bottom of the test section. The mean velocity in the test

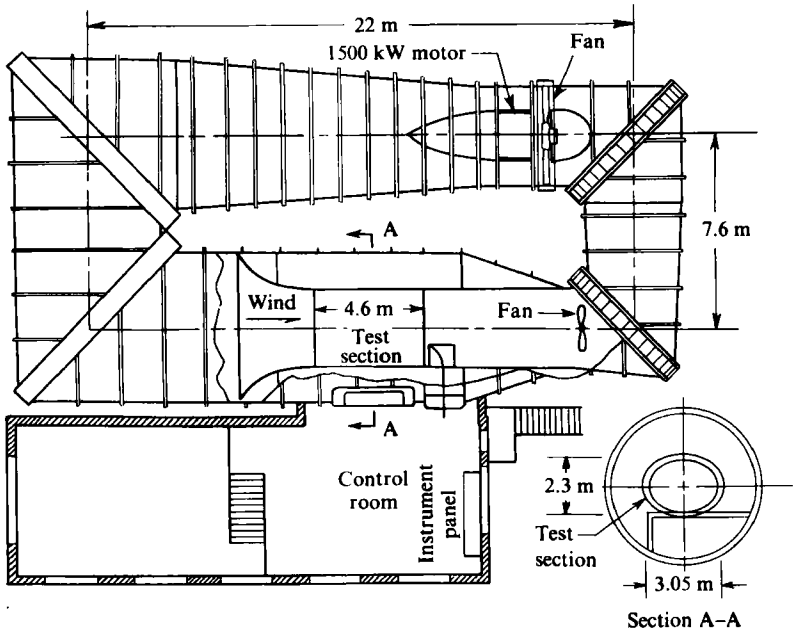

FIGURE 3. Layout of MIT Wright Brothers Wind Tunnel.

section is controlled by either a variable-pitch propeller which can induce velocities up to 80 m/s, or an auxiliary fan suitable for speeds up to 3 m/s.

The flow through the inlet was created by a three-stage centrifugal blower located outside the tunnel. This was designed with backward-leaning blades in order to obtain a large stable-flow range and thereby increase flexibility for parametric studies. The inlet average velocity was determined from the measured pressure drop across a calibrated perforated plate. The maximum value was 135 m/s, so compressibility effects were not significant. Further details concerning the facility are given in Liu *et al.* (1985) and Shin & Shippee (1984).

The inlet model was a circular cylinder with no centrebody, with outside diameter 0.2 m and $D_i/D = 0.75$. The inlet lip was designed to have no separation over the range of conditions of interest using the procedure developed by Boles & Stockman (1977). This yielded an inlet lip geometry composed of elliptical segments.

The nomenclature used in describing the measurements is as follows. Theta (θ) denotes angular position around the inlet. In all tests, the inlet axis was normal to the upstream flow direction, so $\theta = 0°$ is upstream (at the 'leading edge'), $\theta = 90°$ is on the top of the inlet, $\theta = 180°$ is at the rear, and $\theta = 270°$ is at the bottom. This convention applies for both the inner and outer surface of the inlet. The axial coordinate is measured along the inlet axis, with the zero location being at the inlet lip, and the radial coordinate denotes radial distance from the inlet axis.

Two models were machined for the experiments, one of Plexiglas (for flow visualization) and the other of aluminium (for quantitative measurements). Figure 4 shows the aluminium model on its stand, along with the locations of the surface static-pressure taps along the inlet. There are four taps at each axial location, equally spaced around the circumference. During testing, the inlet is rotated around its axis, so that the desired circumferential resolution can be achieved.

Two other aspects of the design of the experiment should also be noted. First,

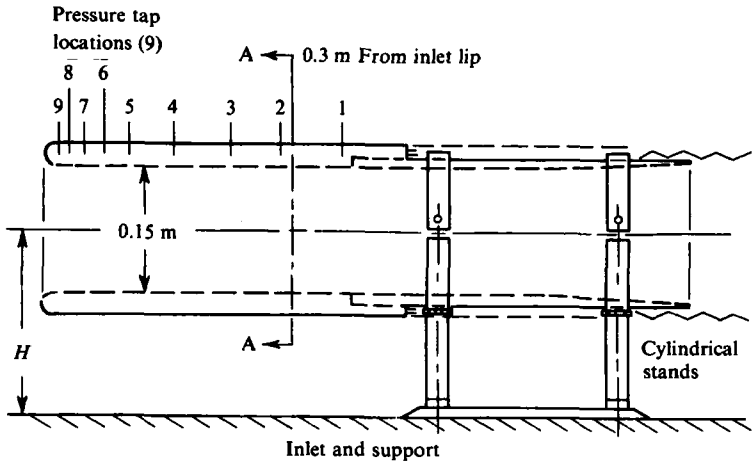

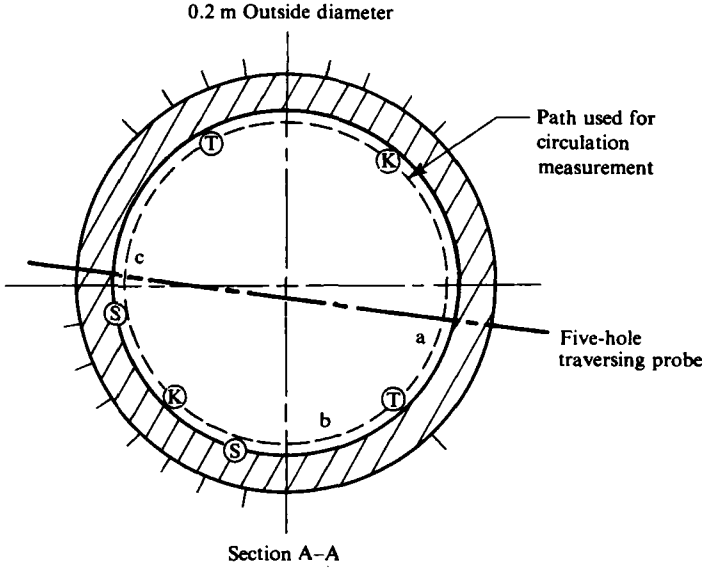

FIGURE 4. Inlet model and measurement stations. T: three-hole probe; K: Kiel probe; S: static tap.

although there is no difficulty in obtaining kinematic similarity between the parameters in the model test and in the actual situation, this is not so for dynamic similarity. In particular, the large size of an actual aircraft engine precludes Reynolds-number similarity for practical model tests. The inlet models were thus equipped with 1.5 mm diameter 'trip wires' at $\pm 67°$ to avoid operation in the transition regime between subcritical and supercritical operation, where the flow depended strongly on small surface-finish irregularities. With these trips, when the model was operated with no flow through the inlet ($CR = 0$) and large H/D, the static-pressure distributions away from the inlet lip were found to be similar to those

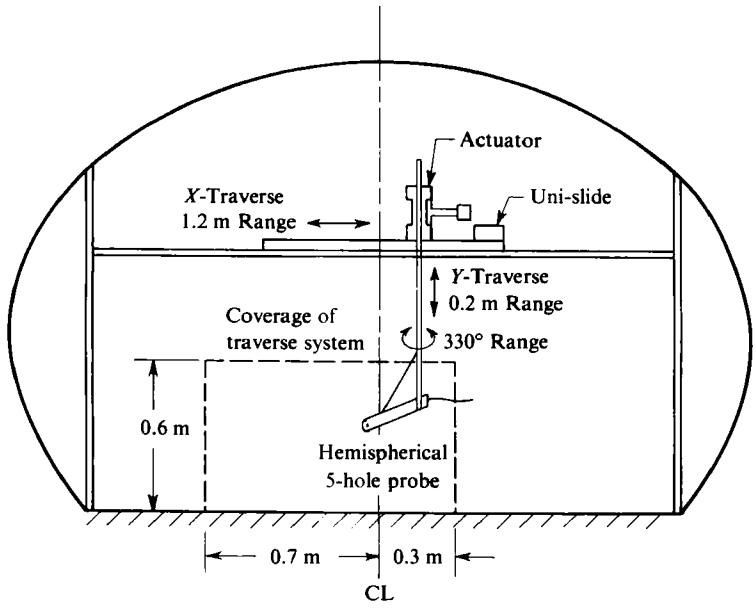

FIGURE 5. Trailing vortex measurement system.

round a circular cylinder at the actual (full-scale) Reynolds numbers of interest. A description of the considerations associated with the use of the trip wires can be found in Shin & Shippee (1984).

Second, the measurements of the inlet-vortex strength were made *inside* the inlet. There were several reasons for doing this. Most important, perhaps, is that it is at the engine-face stations where one really wishes to have the velocity data. Additionally, however, if viscous effects outside of the vortex core are small, the measured circulation will be the same, no matter where one measures it. Thus, if the vortex core is surrounded by fluid which has the free-stream stagnation pressure (which implies negligible effects of viscosity), the station at which the measurements are made is not critical, and it was more convenient to carry out the measurements inside the inlet. Several checks were made on whether the basic assumptions did in fact hold, including one measurement of the circulation around the inlet vortex at a location just below the inlet; these showed that the measurements within the inlet were adequate.

Three-hole and five-hole probes (see figure 4) were used inside the inlet to determine the magnitude of the velocity component needed to establish the circulation around the *inlet vortex*. The measurements were made by rotating the inlet through 360° in 11.25° increments, yielding data at 64 evenly spaced positions around the circumference. A prism five-hole probe was used to make the traverses across the inlet, along path AC indicated in figure 4.

Measurements of the *trailing-vortex* flow field were made 2.5 diameters downstream of the inlet, using a hemispherical five-hole probe. The traverse set-up in the wind tunnel is shown in figure 5. The probe was rotated in yaw and in pitch to stay within the $\pm 30°$ range of calibration. Inlet-vortex circulation measurements carried out at the locations beneath the inlet were done using a single slanted hot wire rotated to three different orientations (Schmidt & Okiishi 1977).

Finally, the position of the core of the inlet vortex was obtained from smoke-flow

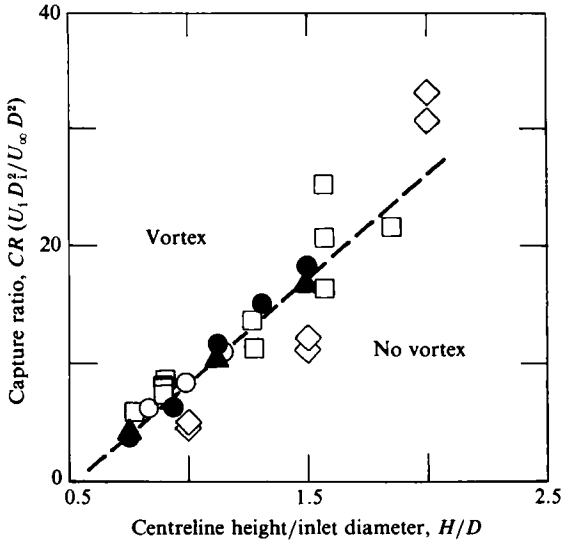

FIGURE 6. Boundaries of vortex/no-vortex regimes. ◇, Motycka; □, Ruehr; ○ Glenney.

Symbol	Source	Conditions
▲	Liu *et al.* (1985)	0.15 m cylindrical inlet, 90° yaw, thick ground boundary layer, $\delta/D \sim 0.8$
●	Present paper	As above except thin ground boundary layer, $\delta/D \sim 0.3$
◇	Motycka, D.L. *et al.* *Pratt & Whitney Aircraft TDM* 2414, 1975	1:11 engine scale model, 135° cross-wind
○	Glenney, D. E., *Aeronautical Research Council C.P.* 1114, 1970	0.15 m and 0.3 m inlets, 55° cross-wind provided by fan
□	Ruehr, W. C., *General Electric Company Report* R75AEG384, 1975	1:16 engine scale model, 60° cross-wind provided by fan, turbofan inside engine model

TABLE 1. Studies of boundaries of inlet-vortex formation

visualization. A plane of laser light was used to illuminate the desired location in the (Plexiglas) inlet. Significant light scattering occurred only in regions of smoke concentration, so that the vortex core could be plainly seen. Since the vortex tended to wander slightly, the technique used to establish the position was to take a number of pictures (a dozen, say) and average the location.

4. Regimes of vortex formation

Before describing the detailed velocity measurements, it is useful to give some description of the regimes in which the inlet vortex is present. Initial measurements of the boundary between the inlet-vortex/no-inlet-vortex regimes were given by Liu *et al.* (1985), but in figure 6 we show not only additional measurements from the present investigation, but also data of several other studies of this phenomenon. The

axes are height-to-diameter ratio, H/D, and contraction ratio, CR. Supplementary information about the different experiments is given in table 1. The points from the present facility, with two different ground-plane configurations having boundary-layer thicknesses differing by more than a factor of two, are plotted as solid symbols. There is essentially no difference between the data from the two configurations, and the dashed line dividing the 'vortex' and 'no vortex' regimes has thus been drawn through all these points.

Several additional comments should be made about figure 6. First, the data from the Pratt & Whitney and General Electric tests were from scale models of aircraft-engine inlets. Second, the data include yaw angles of 55° to 135°. Third, the inlet model sizes did not vary by more than 50% from that used in the present study, so Reynolds numbers were roughly comparable, although none of the other tests made use of a boundary-layer trip. Fourth, out of the available data, only that which was reported to have low values of ambient shear is plotted. Finally, the General Electric tests were done using an axial flow fan to induce the flow through the inlet, so the configuration had a turbomachine and a centrebody.

In spite of these differences, all the data fall fairly closely into a pattern. (The last point would not, in any case, be expected to make a difference.) The presence or absence of the boundary-layer trip does not appear to make much difference as far as the vortex-formation boundary is concerned, although the strength of the vortex, which is not given for any of the other investigations, may be dependent on this feature. Within the data given for the various angles, the yaw angle appears not to be a strong influence, although this conclusion cannot hold all the way to zero-degree yaw (inlet pointing straight into the flow). The general trend is that low values of H/D and high capture ratios tend to promote vortex formation, although, again, this trend will not extrapolate all the way to zero free-stream velocity.

The central point is that the present set of experiments, although carried out on a simple inlet geometry at one value of inlet yaw angle, gives overall flow regimes that are in accord with experiments conducted with more complex (and more realistic) geometries and different yaw angles. The results that appear below will thus be useful, not only as far as shedding light on mechanisms, but also for providing quantitative information for many situations of practical concern.

5. Velocity measurements in an inlet with an (upstream) irrotational crosswind

As stated in the introduction, the features of the vortex system associated with an inlet in cross-wind have previously only been determined qualitatively, and the purpose of this study was to obtain quantitative data on this topic. Specific points to be addressed are the correspondence between the inlet-vortex and trailing-vortex circulations, and the dependence of vortex circulation and position on the capture ratio, CR, and H/D.

The measure of the vortex strength is the circulation, which can be obtained by numerically integrating the velocity around a closed contour enclosing the vortex. Smoke-flow visualization showed the vortex core of the inlet (ground) vortex located near the bottom of the inlet at roughly the 7 o'clock position. The path was therefore a D-shaped one, comprising a constant radius segment (abc) near the wall, and an approximately diametrical part (ca), as is shown in figure 4.

The circulation measurement location was chosen with several constraints: (i) to enclose the vorticity of the inlet vortex only (i.e. not to include streamwise vorticity

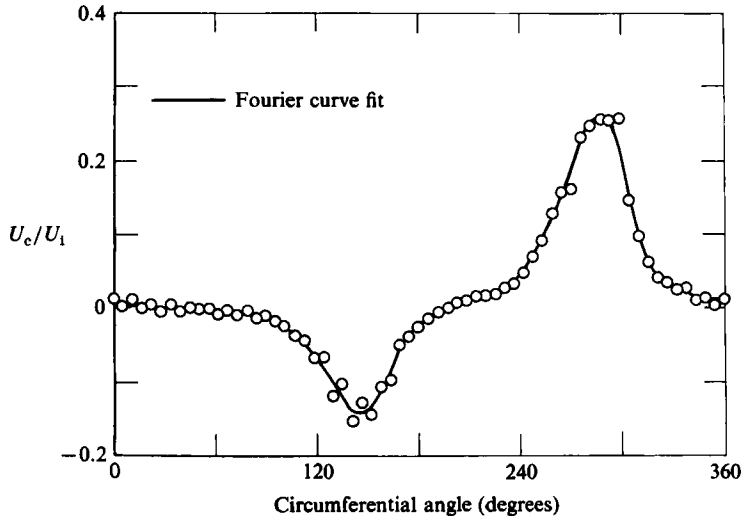

FIGURE 7. Circumferential velocity distribution in inlet $H/D = 1.13$; $CR = 25$; $U_i = 135$ m/s (1.5 D from inlet lip).

resulting from secondary flow in the inlet-wall boundary layer), (ii) to position the probes for the circumferential part of the path close enough to the wall so that pitch angles are small (less than five degrees) and three-hole probes could be used and (iii) to avoid measuring at an axial location where circumferential velocities due to potential-flow effects in the inlet are significant.†

The axial location chosen was 1.5 diameters (2 inner diameters) from the lip, since at this distance the above effects are small (Shin & Shippee 1984). Turbulent-boundary-layer calculations give an estimate of the boundary-layer thickness at this location as 6 mm (displacement thickness 0.7 mm). Further, (two-dimensional) potential-flow calculations of flow due to a vortex in a circular inlet, using the estimates of vortex strength developed in Liu *et al.* (1985) and the vortex position from flow visualization, imply that the pitch angles would be within the desired range at this position. The circumferential part of the contour was thus 174° of a circular arc at a radius of 0.92 inlet inner radius.

To show the main features of the circumferential velocity due to the inlet vortex, figure 7 presents the non-dimensional circumferential velocity, U_c/U_i, along this contour, for a condition of $H/D = 1.13$ and $CR = 25$. Each point on the plot represents the average of three runs. Experimental uncertainty for each of these (and other circulation measurements) was estimated at ± 10 per cent. Although only the circumferential velocity between the angles of 191° and 5° is necessary for the circulation calculation, the velocity field over the rest of the circumference is of interest in developing a picture of the general flow field in the inlet.

A striking result is the existence of *two* areas of high circumferential velocity,

† Near the inlet lip, the flow has to turn into the inlet. The streamline curvature brings with it a consequent cross-stream pressure gradient and hence circumferential-velocity non-uniformity. At locations away from the lip inside the inlet, however, the axial velocity is constant over an annular region (or would be, if there were no inlet vortex). As one moves into the inlet from the lip, therefore, there must be significant circumferential velocities associated with the redistribution of flow over the annulus. Trying to measure the circulation in the presence of such effects essentially means trying to take the difference of two large numbers, and it is desirable to avoid such a situation.

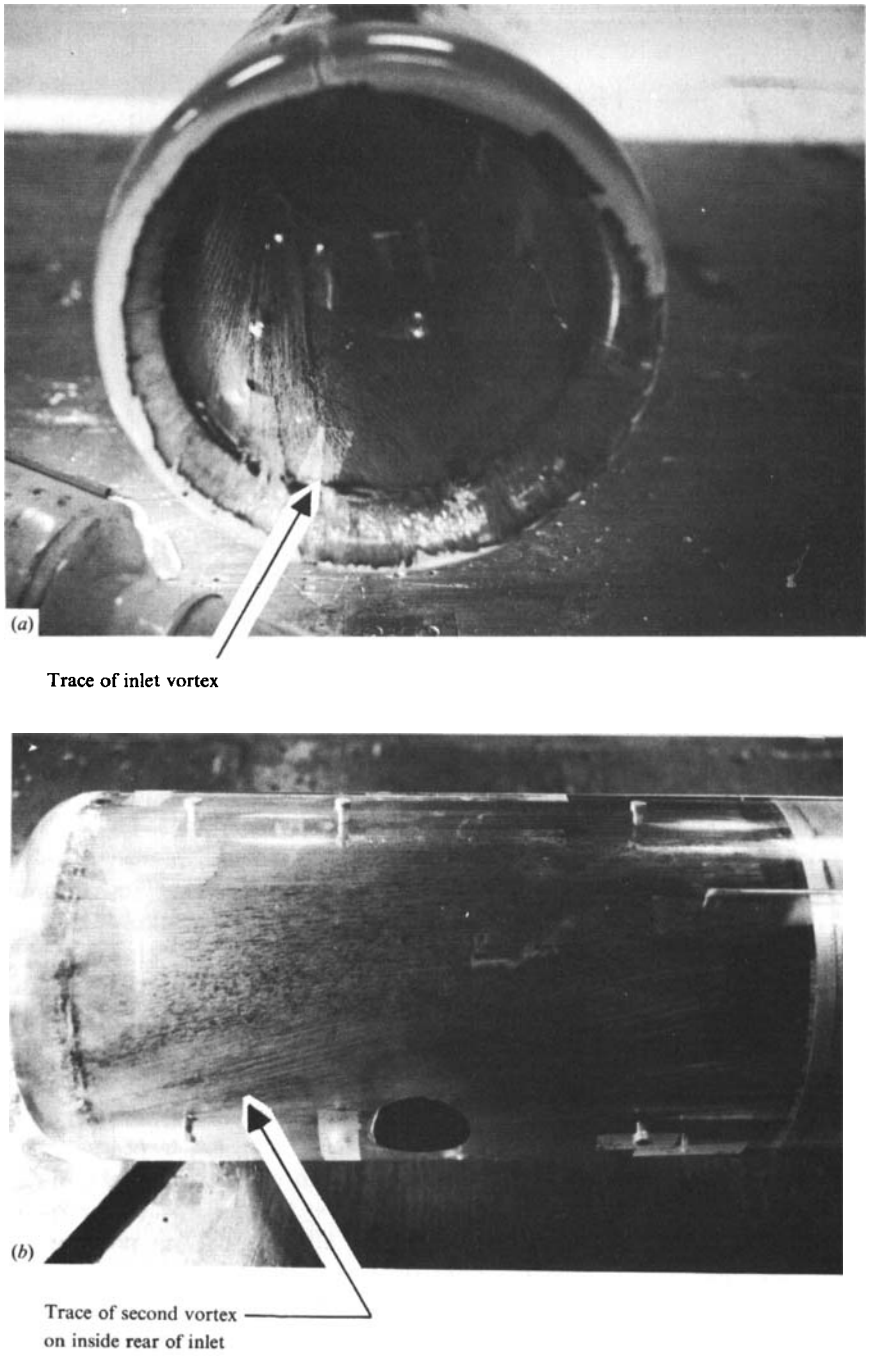

FIGURE 8. Lampblack surface flow visualization (*a*) inside inlet, and (*b*) outside rear of inlet.

indicating *two* vortices in the inlet. One, centred near 280 degrees, is the 'inlet vortex'. The other, which has not been previously observed, and which has a circulation *opposite* to that of the inlet vortex, is centred at approximately 150 degrees (roughly '2 o'clock'). The vorticity field associated with this second region will be discussed subsequently.

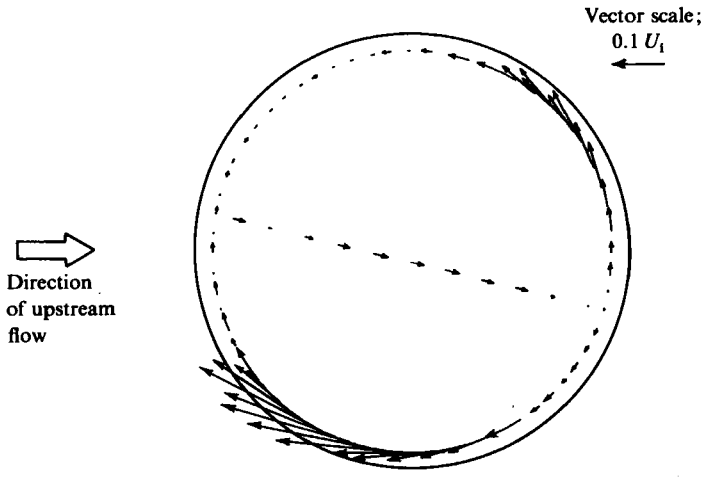

FIGURE 9. Cross-plane velocities inside inlet. $H/D = 1.13$; $U_i = 135$ m/s; $CR = 25$ (1.5 D from inlet lip).

To complement the velocity measurements, lampblack-flow visualization was used on the inside surface of the Plexiglas inlet, and the results are shown as figures 8 (*a*) and (*b*). In figure 8 (*a*), the lampblack streaks originating at 270 degrees near the lip shift to roughly 300 degrees at two diameters from the lip, showing that the lower vortex moves clockwise as one proceeds into the inlet. This is due to the interaction (of the vortex) with the inlet wall, as can be readily seen by considering the velocity induced by the appropriate image vortex. The lampblack traces due to the second vortex are shown in figure 8 (*b*). The streaks originate at about 150 degrees at the lip and move, again in accord with image-vortex arguments, to a location, roughly 5–10 degrees counterclockwise at two-diameters from the lip.

A vector plot of the velocity components along the contour of integration is shown in figure 9, which is a view looking into the inlet with the free-stream velocity coming from the left. The ground plane is not shown, but it is below the inlet. It can be seen that by far the more important contribution to the circulation integration is from the circumferential velocity along the circular arc. This is also indicated from potential-flow calculations of the velocity field due to two vortices inside a circular cylinder. Since the vortices are close to the boundaries, the region over which the velocities are large, which is of the scale of (say roughly twice) the vortex–image-vortex separation distance, is thus also rather localized.

The assumptions concerning probe position can also be examined. The requirements that the probes be out of the boundary layer and at a location where the potential-flow effects are small correspond to a situation in which the stagnation pressure is constant and the static pressure shows only a small local depression due to the presence of the vortex. Figure 10 shows representative pressure distributions around the inside of the inlet. The static pressure can be seen to be as desired; however, the stagnation pressure shows two regions having mild defects. One is near 100 degrees, outside the contour used for the circulation measurement, and is thus not of concern for this measurement. The other region, however, is near 300 degrees, and therefore does affect the circulation measurements.

Potential-flow calculations imply, and flow visualization bears out, that the regions of low stagnation pressure are due to the convection of boundary-layer fluid by local radial velocities induced by the vortex. The boundary-layer accumulation occurs on

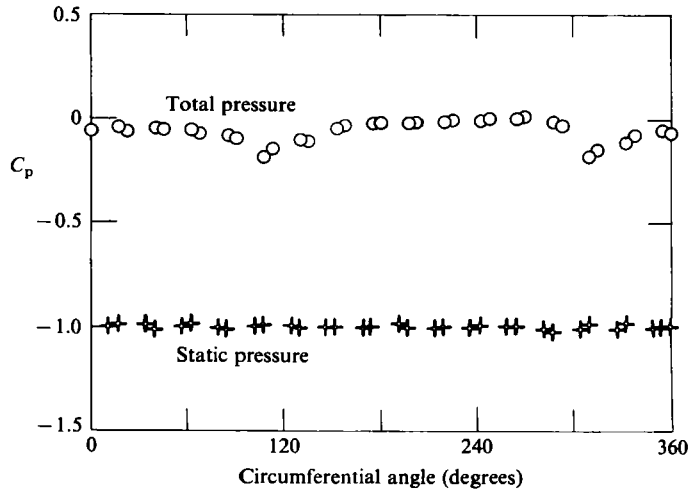

FIGURE 10. Total and static pressure distributions in inlet $C_p = 2(P-P_\infty)/\rho U_1^2$.

opposite sides of the vortices (at a larger circumferential angle for the lower vortex and at a smaller angle for the upper vortex) in accordance with the respective circulation of each.

If there is significant flux of vortical fluid from the boundary layer into the contour, the measured circulation of the inlet vortex will be affected. One can, however, make (crude) estimates of the influx of vorticity associated with the radial inflow; doing this leads to the conclusion that the effect is small. An additional demonstration can be made by carrying out the measurements at a different axial location, and this was done at a station one diameter, instead of 1.5 diameters, from the lip. While the measured circulation at this upstream location was slightly larger (7 %), the differences were less than the estimated experimental uncertainty. Hence the above effect is not significant for the conclusions of the present study.

There were, however, differences in two aspects of the velocity measurements at the two axial locations. First was a shift of approximately 10 degrees in the angular position of the peak circumferential velocities. As described in connection with the flow visualization, this is consistent with potential-flow estimation of the lateral drift of a vortex near a wall. Second, the stagnation pressure defects were slightly less at the upstream location, as one would expect, since radial transport has had less distance over which to act and boundary layers are thinner.

As a check on the circulation measurement inside the inlet, the circulation around the ground vortex outside the inlet was also measured using a slanted hot wire for several different (horizontal) rectangular contours below the inlet lip. The circulation obtained in this manner was approximately 75–80 % (depending on the specific contour) of that obtained from the measurements inside the inlet. The values measured inside the inlet are preferred, however, because of the uncertainties associated with the ground-vortex measurement. These uncertainties included the strong three-dimensionalities of the flow at the measurement locations, the fact that the circulation integration involved, in part, taking the difference due to the opposite velocity contributions along the contour, and the unavoidable situation of the ambient boundary-layer thickness being comparable to the height at which the measurements could be made. In view of these, the agreement is considered adequate.

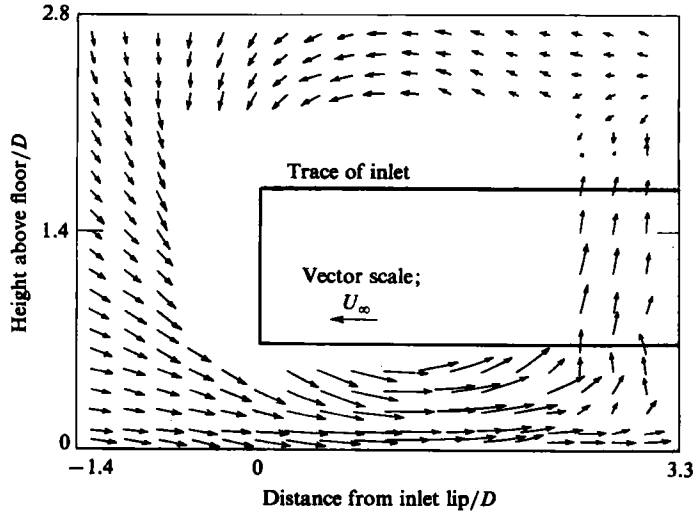

FIGURE 11. Cross-plane velocities in trailing vortex $H/D = 1.13$; $CR = 25$.

Although some parametric information will be given subsequently about the inlet-vortex circulation, at present we wish to pursue only the verification of the hypothesis concerning the inlet-vortex and trailing-vortex circulation. In this context, we can thus summarize: for CR of 25 and H/D of 1.13, which were the values at which we measured the trailing vortex (described in the next section), the measured non-dimensional inlet-vortex circulation, $\Gamma/U_\infty D$, was 5.5.

6. Trailing-vortex measurement

The trailing-vortex circulation was measured at conditions with a strong inlet vortex: $H/D = 1.13$, and $CR = 25$. The circulation was calculated from velocities in a plane downstream of the inlet, perpendicular to the direction of the far upstream flow. Again, there were several conflicting constraints on the location of the measurement station. It was desirable to have a region of 'freestream' flow between the trailing vortex and the ground boundary layer; this limited how far back the traverse plane could be. Against this, however, it was useful to have a clearly defined trailing vortex for ease of measurement, and establishment of this type of structure took several diameters. After (considerable) smoke-flow-visualization studies, a location three diameters downstream was selected as optimum.

Cross-flow velocity vectors, which represent a 12 s time-average value, are shown in figure 11, with the velocity vectors as seen-looking upstream towards the inlet. The trace of the inlet is also given in the figure. The region in the middle of the figure was not measured, since it is only the velocity vectors on a contour enclosing the vortex that are needed.

The circulation round the trailing vortex obtained from these measurements has the same magnitude as that found for the inlet vortex, $\Gamma/U_\infty D = 5.5$, the difference between the measurements being within the experimental uncertainty. In addition, as can be seen from a comparison of figures 9 and 11, the sense of the inlet-vortex and trailing-vortex circulations is opposite. Thus, as hypothesized, the inlet and trailing vortex are opposite in sign and essentially equal in magnitude.

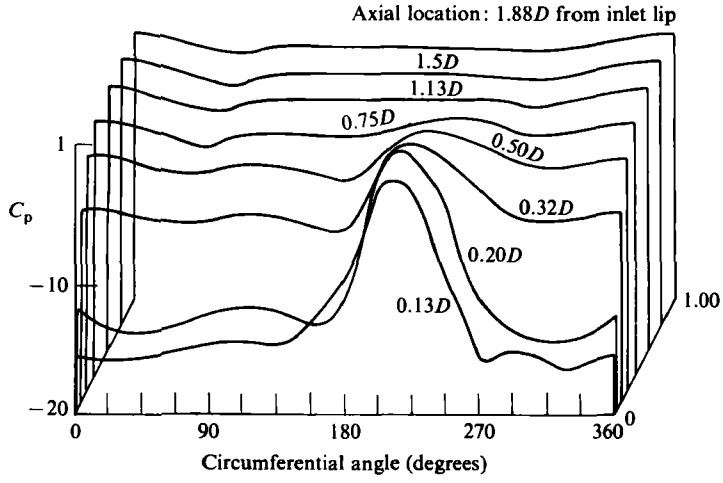

FIGURE 12. Static pressure distribution on inlet surface.

7. Inlet circulation far from the lip

An implied part of the above hypothesis is that the circulation round the inlet at locations far from the inlet lip is small. This is certainly plausible, since the velocities on the outer surface of the inlet are on the order of U_∞ there and, hence, much lower than those near the lip. We can examine this in a bit more detail using data on the static-pressure distribution round the inlet. This is plotted in figure 12, which shows curves of static-pressure coefficient, $C_p(=(P-P_\infty)/(P_T-P)_\infty)$, on the inlet outer surface versus circumferential position, for axial locations ranging from 1.88 diameters to 0.13 diameters from the inlet lip. Conditions are the same as those for the inlet-vortex and trailing-vortex measurements. Figure 12 extends the data given by Liu *et al.* (1985) to a substantially higher capture ratio.†

At the locations far from the lip (at $1.5D$ and $1.88D$, say), the trough in the curve of static-pressure coefficient has a value near -1, and is roughly symmetric about $\theta = 0°$. These two features of the static-pressure distribution imply that the circulation is small. The circulation can be estimated using the measured static-pressure distribution, neglecting the small component of flow *along* the inlet. In carrying out this calculation, one also has to estimate where the flow separates at the rear of the inlet, but: (i) the static pressure distribution is such that one can make this estimate with a reasonable degree of confidence (see below), and (ii) the conclusion about the magnitude of the circulation is unchanged using any plausible estimate of separation location.

Since the location of the minimum velocity is very close to $\theta = 0°$, an estimate of the non-dimensional (clockwise) circulation can be expressed as:

$$\Gamma/U_\infty D = \frac{1}{2}\left[\int_0^{\theta_{sep+}} (1-C_p)^{\frac{1}{2}}\,d\theta - \int_0^{\theta_{sep-}} (1-C_p)^{\frac{1}{2}}\,d\theta\right],$$

† It is not the intent here to present a general discussion of the features of the static-pressure distribution, since these have been examined in Liu *et al.* (1985). It was shown there that the static-pressure distribution at both high (as shown here) and low values of capture ratio can be clearly interpreted in terms of the interaction between an overall flow into the inlet and the inlet-/trailing-vortex system.

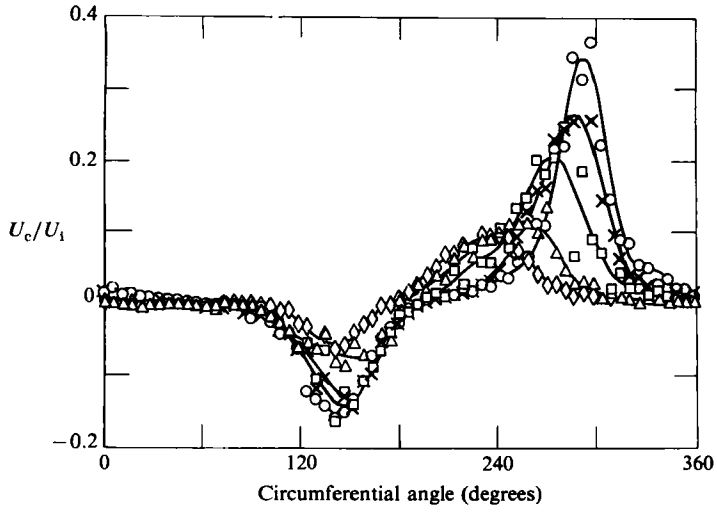

FIGURE 13. Effect of H/D on circumferential velocity distribution in inlet; $CR = 25$. ○, $H/D = 0.75$, vortex; ×, 1.13, vortex; □, 1.31, vortex; △, 1.43, vortex; ◇, 1.50, vortex.

where the notation $\theta_{\text{sep}+}$, $\theta_{\text{sep}-}$ denotes upper and lower separation locations at the rear of the inlet. (For reference, at the $1.88D$ axial station these are at $\theta = 101$ degrees and 237 degrees respectively – the static-pressure coefficient is virtually flat between these locations, varying by less than ± 0.02.) The calculated circulation round the inlet at the $1.88D$ location is less than $0.2U_\infty D$, i.e. less than five per cent of either the inlet vortex or the trailing vortex, thus confirming this aspect of the conceptual picture that has been developed.

8. Effects of capture ratio and H/D on vortex strength and position

To investigate the influence of capture ratio and inlet height-to-diameter ratio on vortex strength and position, a limited parametric study was carried out. To show the influence of the height-to-diameter ratio, the velocity fields in the inlet were measured at $H/D = 0.75$, 0.94, 1.13, 1.31, 1.43 and 1.50, keeping a constant value of $CR = 25$. To examine the effects of the capture ratio, measurements were carried out at $CR = 2.3$, 10 and 25, at a value of H/D of 0.75. (The capture ratios of 2.3 and 10 were chosen since inlet surface static pressure data had been previously taken by Liu at these values.) The velocity measurements were made in the inlet at the axial station 1.5 diameters from the inlet lip.

Figure 13 shows the circumferential velocity as a function of circumferential position for five values of H/D: 0.75, 1.13, 1.31, 1.43, 1.50. The curve for $H/D = 0.94$ is not plotted (to help figure clarity) but it was virtually the same as that for $H/D = 0.75$. (This curve, as well as other data referred to here, can be found in Shin & Shippee 1984.) The figure clearly indicates that the circulation of the inlet vortex decreases in strength as the height-to-diameter ratio is increased. The change in shape of the curve also implies a qualitative change in the position of the vortex; this will indeed be seen below to be the case. What has in fact occurred, as can be seen by the broadening of the velocity distribution, is that the vortex at the higher values of H/D has moved away from the inlet wall.

The effect of decreasing the capture ratio (at a constant H/D of 0.75) is shown in

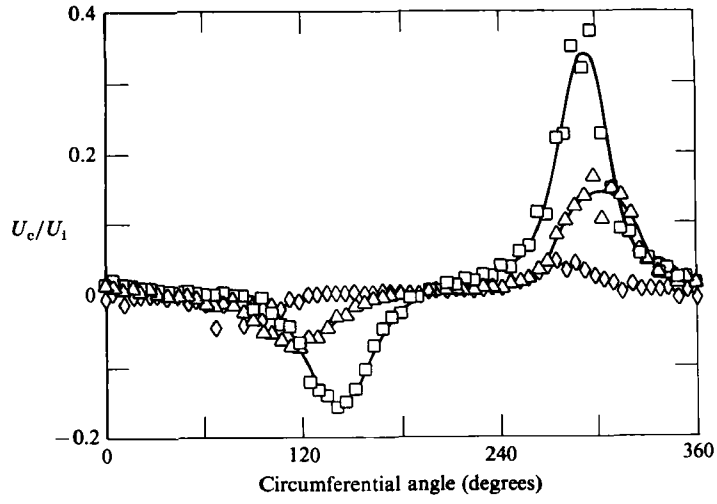

FIGURE 14. Effect of contraction ratio (CR) on circumferential velocity distribution in inlet; $H/D = 0.75$. □, $CR = 25$ vortex; △, 10 vortex; ◇, 2.3 no vortex.

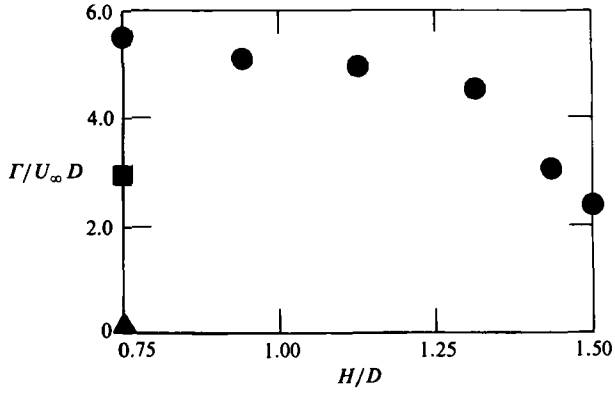

FIGURE 15. Variation of inlet vortex strength with H/D and CR. ●, $CR = 25$; ■, 10; ▲, 2.3.

figure 14. Decreasing the velocity ratio reduces the inlet-vortex strength (this trend is similar to that observed with increasing H/D) but results in a shift of the position of maximum circumferential velocity in the opposite direction from that seen with increasing H/D.

The overall effect of these parametric changes on the vortex circulation is shown in figure 15, which gives the non-dimensional circulation, $\Gamma/U_\infty D$, for all of the points at which data was obtained. The circulation is a strong function of CR. At a constant value of $CR = 25$, over the range of H/D from 0.75 to 1.25, say, which represents current wide-bodied jets, the circulation is roughly constant (~ 5); however, as H/D increases from this latter value, the circulation drops off sharply.

The location of the core of the inlet vortex inside the inlet was determined using smoke introduced into the vortex near the ground. The results are presented in figure 16. An obvious feature is the large change in the position of the vortex between $H/D = 1.5$ and the other values of H/D for a capture ratio of 25. This is consistent with the qualitative change in the nature of the circumferential-velocity distribution

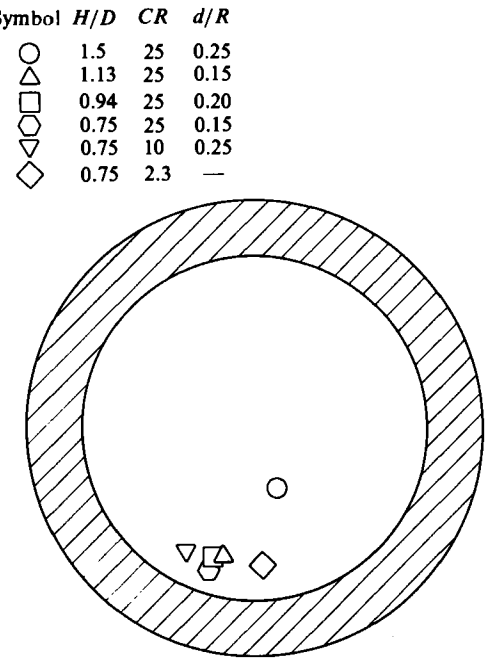

FIGURE 16. Vortex-core location with H/D and CR; d is core diameter; $R_1 = 0.075$ m.

which has been previously discussed. Note, however, that an inlet vortex still existed at this condition.

9. Flow regimes and structure of the vorticity field

9.1. *Three-dimensional vorticity field near the inlet*

Figure 2 showed a very simplified picture of the connection between the inlet vortex and the trailing vortex, based on arguments concerning the constancy of circulation along a vortex tube. We now return to this point and describe in more detail the pattern of the vortex lines, both inside and outside the inlet, in the region near the inlet lip. This has been inferred from (i) detailed flow-visualization studies of the flow field, using smoke, and (ii) examination of the limiting streamlines on the outer surface of the inlet, using the technique described by Langston *et al* (1982). (In this technique, ink dots are placed on a sheet of Mylar, which has been laid on the surface to be studied. When sprayed with oil of wintergreen (methyl salicylate), the dots flow under the action of the surface shear stress.)

In considering the vorticity field there is an important distinction to be made between the flow downstream of the inlet in the present situation and that in may other trailing-vortex flows. At the high values of capture ratio that typically characterize an inlet vortex, there is a very strong sink effect associated with the flow into the inlet. This effect dominates in the neighbourhood of the inlet lip and therefore has important implications concerning the trailing vortex.

In situations such as a finite wing, for example, vorticity is fed into the trailing vortex from the (spanwise flow in the) boundary layers on the body. This vortical fluid leaves the body at the trailing edge (for a well designed wing at design conditions)

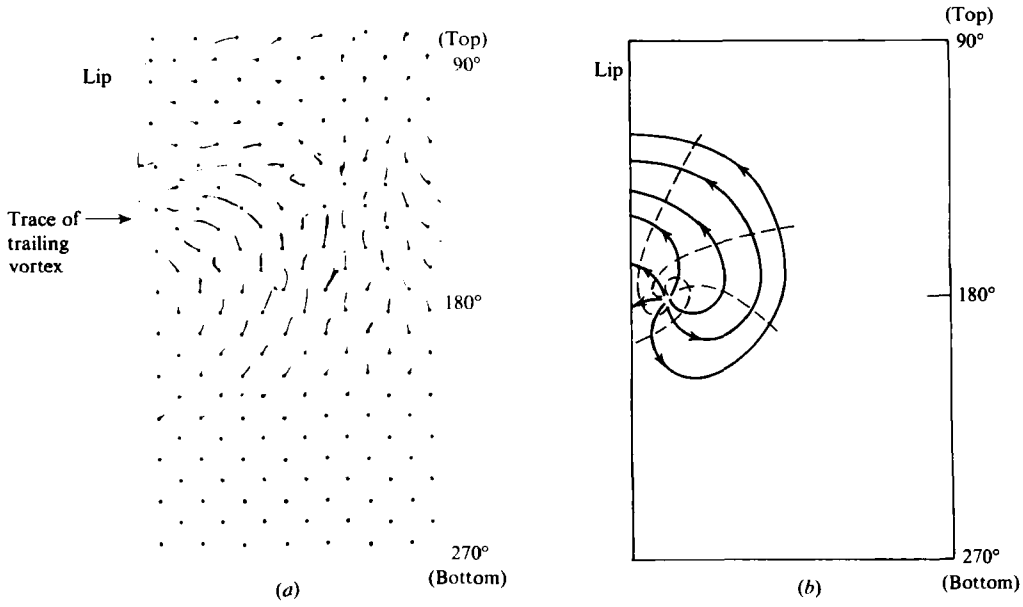

FIGURE 17. Inlet surface flow-visualization results. (*a*) Surface flow visualization using ink-dot wintergreen technique of Langston *et al.* (1982). (*b*) Sketch of limiting streamlines (solid) and surface vorticity vectors (dashed) on rear of inlet.

and is convected downstream. In the present situation, however, this is *not* the case. Near the inlet (up to a diameter or so downstream, depending on capture ratio), the flow in the trailing vortex is *upstream*, towards the inlet. This means that there is no flux of vorticity into the trailing vortex from the boundary layers on the inlet surface, but that vortical fluid is, in fact, flowing *from* the trailing vortex *onto* the rear surface of the inlet. Surface flow visualization and observation of smoke patterns show that there is a focus of *attachment* (e.g. Lighthill 1963; Tobak & Peake 1982) on the rear of the inlet, near 180 degrees and within a distance of approximately one-quarter diameter from the lip. (This behaviour can be contrasted with the flow in the inlet vortex, which exhibits a focus of *separation* on the ground plane.)

The results of the surface flow visualization are presented in figure 17, which shows the rear of the inlet surface from close to the lip to a diameter away. The left-hand side (*a*) shows the ink-dot visualization traces. (The region very close to the lip is not shown, as this technique could only be used successfully at a distance greater than approximately $0.1D$ from the lip.) Although the flow pattern is complex, due to the strong axial flow along the inlet surface, the trace of the trailing vortex is clearly visible. The figure on the right is a sketch of the limiting streamline pattern (the solid lines) which might be inferred from the flow visualization. The dashed lines in this figure give an indication of the surface vorticity vectors, which are perpendicular to the limiting streamlines (Lighthill 1963; Tobak & Peake 1982; see also Maskell 1955).

The vorticity pattern off the surface is shown in figure 18, which presents a top view of the trailing-vortex system. Because vortex lines cannot end in the fluid or on a stationary surface, the vortex lines in the core of the trailing vortex must be as sketched. Some of the vortex lines in the trailing vortex thread through the boundary layer on the outer surface of the inlet before entering the inlet, for example the lines close to E, which is near the location of the focus of attachment. Others,

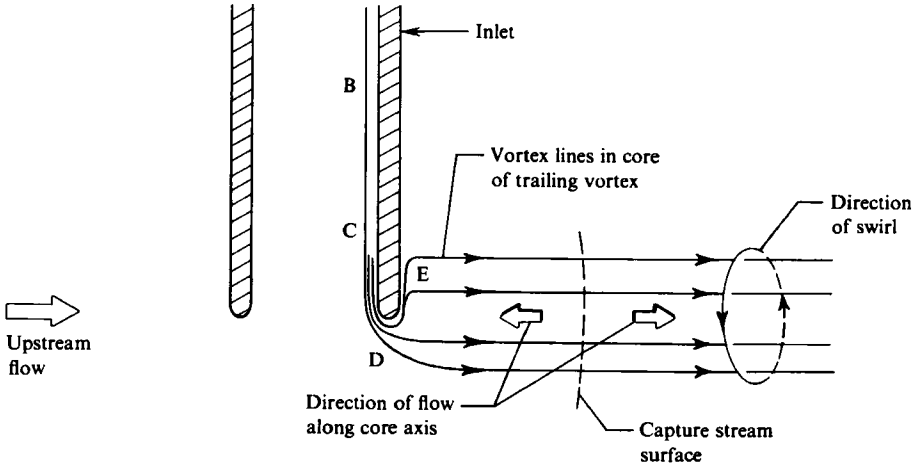

FIGURE 18. Top view of vortex lines in trailing vortex and flow in vortex core.

however, are not associated with the boundary layer but are ingested directly into the inlet, for example the lines near D. Note that the flow in the trailing vortex is *upstream* near the inlet; this aspect will be discussed in the next section.

The fact that some of the lines must thread through the boundary layer can also be inferred from the static pressure distribution along the inlet shown in figure 12. The variation of the C_p distribution with axial location implies that, as stated in §1, the circulation is changing along the inlet and that (at least for the wide range of capture ratios investigated) almost all of this change is occurring within half a diameter of the lip. This, however, is the region in which the visualization shows that the trailing-vortex flow attaches to the rear of the inlet.

We can also interpret the distribution of circumferential velocity measured inside the inlet in terms of these ideas. The main contribution to the circulation about the two D-shaped contours indicated in figures 4 and 9 is from the circumferential velocity. It can be seen from figures 7, 13 and 14 that the circulation around the inlet vortex (represented by the circumferential velocity from 191 to 5 degrees) is roughly twice that associated with the second region of axial vorticity which was found at the upper rear of the inlet. The reason is that the contour around which the measurements were carried out does not include all the axial vorticity in the latter region, which may extend very near to the wall. Put another way, the net circulation due to the inlet vortex and to the vortex filaments that come from the trailing vortex should be zero.† The reason that there is a measured net circulation is that, although the contour used in the measurement does enclose all the vortex filaments associated with the inlet vortex, it does not enclose all the vortex filaments that enter the inlet from the trailing vortex.

† It is of course true that, because the velocity at the walls is zero, the net amount of axial vorticity inside the inlet, i.e. the circulation, is always zero. For example, the circumferential-velocity distribution in figure 7 implies that there is a net amount of axial vorticity in the boundary layer, from 191 to 5 degrees, on the inside of the inlet which is essentially equal and opposite to that in the inlet vortex. This vorticity, however, has been diffused from the inlet wall. The above arguments refer to the vortex filaments that are convected into the inlet, rather than to vorticity which has been diffused from the walls within the inlet.

9.2. *Flow in the trailing vortex downstream of the inlet*

The discussion so far has been of the flow in the neighbourhood of the inlet lip. Further downstream, say two diameters, the flow in the trailing vortex is in the downstream direction, as indicated in figure 18. This implies that there must be a region where the component of velocity in the downstream direction is zero. This marks part of the 'capture surface'. Fluid particles upstream of this are ingested into the inlet whereas particles downstream are convected downstream, as indicated by the bold arrows on figure 18.

The existence of this region has an important consequence as regards the question of the origin of the vorticity in the core of the trailing vortex. Based on the above observations, the conclusion is that the vortex lines in the core are maintained through *production of vorticity by vortex stretching* rather than by convection of vorticity into the core. To state this in a different manner, the fluid that enters the core (and flows upstream and downstream) does so from the irrotational flow that came over and under the inlet. This fluid is entrained into the core, so that (viewed on a local basis) it is (turbulent) diffusion along the outer boundary of the core which imparts the vorticity to the fluid that enters the core.

This basic process was described in some detail in DS, where the application was to the (ground-to-)inlet vortex and to vortices that stretched from one inlet to another, surrounded by irrotational flow. The flow visualization shows, however, that the same considerations apply to the trailing vortex.

Note that all the vorticity present in the core must have been produced initially by the action of viscosity during the 'startup transient' of the vortex system. (For concreteness, one can think of this as the initial evolution of the flow that occurs when the blower is turned on.) During this transient, the vortical fluid can only come from the boundary layers on the outside of the inlet. Once formed, however, analogous to the phenomenon described in DS, there is no need for any further vorticity to be convected into the core, and the flow visualization appears to bear this out. The steady-state condition thus represents a balance between vorticity production (due to the strong stretching associated with the stagnation region) and diffusion; as in DS, consideration of the transient process is vital for understanding of the steady-state flow.

9.3. *Relation between inlet and trailing vortices*

An overall view of the relation between inlet and trailing vortices is shown in figure 19. The inlet vortex is at A (the parts of the vortex filaments which thread into the ground boundary layer are not shown for clarity). The vortex lines in the inlet vortex continue into the inlet, as at B, with the direction of the vorticity vector as shown. The vortex lines associated with the inlet vortex must join 'at infinity' with the vortex lines in the trailing vortex; however, the exact manner of this joining is not critical to events in the region of interest and is not shown. The vortex filaments at C are those which appear in the vortical region at roughly two o'clock inside the inlet, and the circulation around these vortex filaments and the inlet vortex is essentially equal and opposite.

As indicated, the vortex lines at C continue out of the inlet. Some thread through the boundary layer on the outer surface of the inlet (near E), before going into the core of the trailing vortex, while others go into the core without going through the boundary layer (near D). As emphasized above, although the vorticity vector points downstream, the direction of flow near the inlet on the downstream side is actually

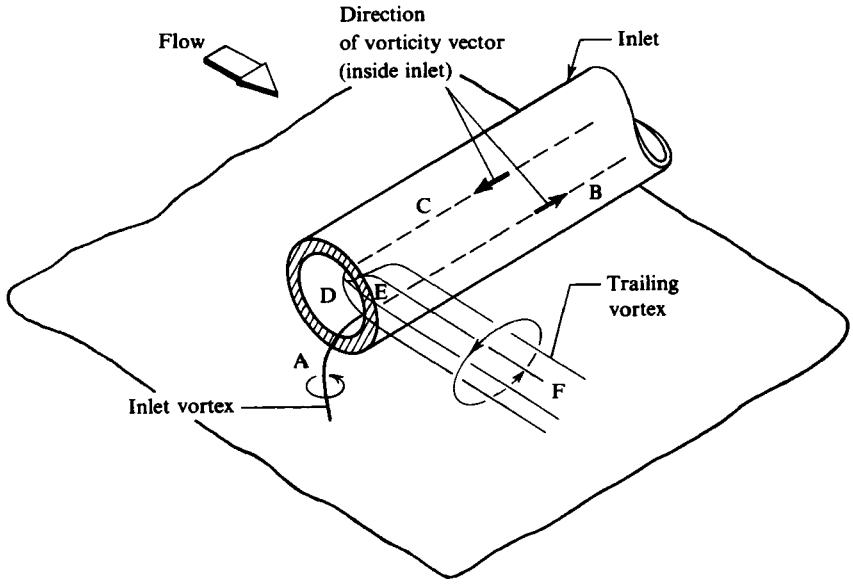

FIGURE 19. Vortex lines in inlet and trailing vortices.

upstream. Finally, the overall direction of the swirl in the trailing vortex (F) is also indicated.

The picture that has been presented is more detailed and also more complex than that given in § 1. In particular, it appears that a key feature of the flow – the strength of the inlet vortex circulation – although connected with the circulation variation along the inlet, cannot be directly related to it. In other words, the net amount of vorticity that appears in the boundary layers on the outer surface of the inlet is set by the difference between the circulation round the inlet vortex and that round the trailing vortex filaments which enter the inlet *without* threading through the surface boundary layer. This is quite different from the situation with a solid body, such as a wing, in which all the trailing vorticity comes from the boundary layers on the wing surface. The difference is fundamental to devices (such as inlets) with large capture ratios where one is interested in the aspects of the flows, not only outside but also inside the device.

9.4. *Flow regimes and overall vortical structure*

Using the information obtained about the flow in the vortex core, we are now in a position to examine some of the more global features or 'skeleton' (Perry 1981) of the vortical structure. The description that follows has been obtained using flow visualization in the wind tunnel, as well as the hydrogen-bubble technique in a water tunnel.

As a framework for describing the vorticity field, we can consider the flow regimes encountered with an inlet operating near the ground plane as the capture ratio, CR, is increased. The inlet is in cross-wind in a flow that is uniform far upstream.

With no inlet velocity, $CR = 0$ (no flow into the inlet), the inlet is essentially a semi-infinite cylinder. There are vortex layers shed from the top and bottom of the inlet and from the end of the inlet. The vortex filaments in these layers are shown schematically in figure 20 (a). They are depicted as straight for simplicity, although it is recognized that the actual configuration is more complex.

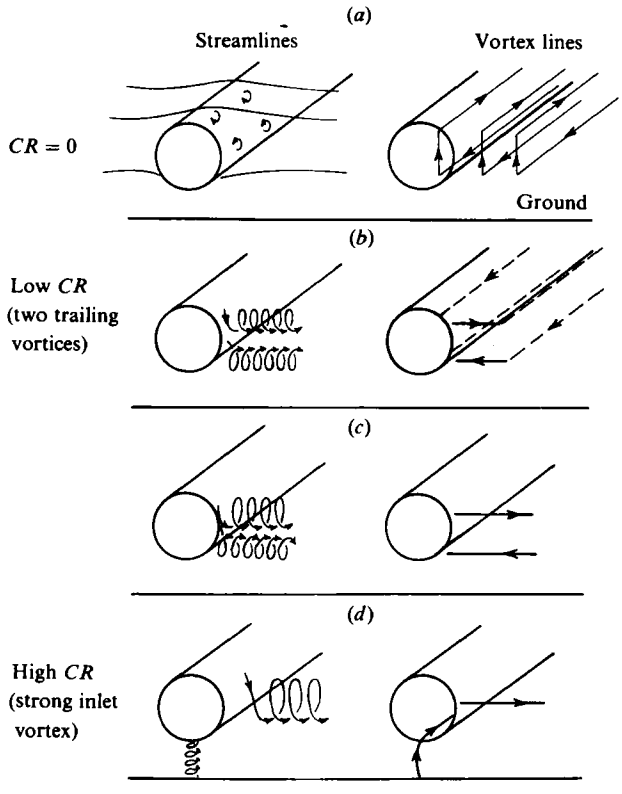

FIGURE 20. Schematic of variations in flow regime as CR is varied.

As the capture ratio is increased from zero to a low value (between one and five, say) two distinct trailing vortices form (figure 20*b*). As described in the previous section, near the rear of the inlet lip, the swirling flow associated with the cores of these vortices is sucked into the inlet. The streamlines are sketched at the left where, for clarity, we have not drawn the details of the flow near the lip.

As the capture ratio increases, the trailing-vortex system shifts downward counterclockwise, as indicated in figure 20(*c*), with the upper vortex increasing in diameter and the lower one decreasing. The circulation around each vortex increases, although it remains essentially equal and opposite for the upper and the lower one. As the capture ratio is increased still further, the lower vortex shifts abruptly to attach to the ground, forming the inlet vortex (figure 20*d*).

This shift was examined in detail in the water-tunnel experiments. As the capture ratio was (very) gradually increased, the two trailing vortices exhibited considerable lateral, as well as up and down, movement, with the lower vortex intermittently attaching to the ground. A slight increase in capture ratio then caused a strong, stable, inlet vortex system to suddenly appear. Increasing the capture ratio further from this value resulted primarily in a decrease in the core size, as might be expected from consideration of the balance between convection and diffusion that occurs in the core, and a small upstream movement of the core.

The abruptness of the transition between the two states was suggested by Marble (personal communication) from consideration of the kinematics of trailing vortices in an inviscid fluid. The basic argument is that the lower trailing vortex cannot simply

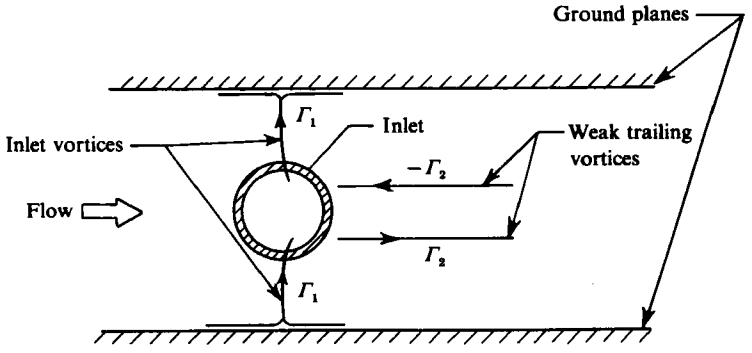

FIGURE 21. Schematic of vorticity field for inlet between two ground planes.

move down until it touches the ground (at a far downstream location) and then, if capture ratio is increased, move gradually upstream. Rather, once it touches the ground, the high (infinite for a line vortex) induced velocities at the point of contact result in a very rapid motion of this point, initially at right angles to the upstream flow and then upstream, leading to the formation of the inlet vortex configuration described.

The transition from an inlet vortex to the two trailing vortices, when the velocity ratio was decreased, also occurred quite abruptly. It was observed that waves first appeared on the core of the inlet vortex. As the velocity ratio was then lowered past a critical point, the vortex was shed downstream and the configuration with two trailing vortices appeared.

The observed shift of the lower trailing vortex to attach to the ground gives rise to an interesting question concerning the upper of the trailing vortices (Marble, personal communication). This is whether, in the presence of a second ground plane placed symmetrically above the inlet, the upper trailing vortex would attach to the top ground plane, leaving *no* trailing vortex. While we could not pursue this in any depth, we did carry out some exploratory flow-visualization studies of such a configuration, and the results are sketched in figure 21. A strong vortex was indeed formed from the top plane to the inlet. It was also found, however, that two weak vortices trailed from the rear of the inlet. No measurements were taken of circulation but, based on the flow visualization, these trailing vortices were clearly much weaker than the two inlet vortices.

10. Summary and conclusions

1. Detailed measurements and flow visualization have been carried out for an inlet operating near a ground plane. The purpose was to obtain quantitative information on the structure of the three-dimensional flow field associated with an inlet vortex.

2. Height-to-diameter ratio H/D, and capture ratio $CR(= U_i D_i^2 U_\infty D^2)$ were varied over a wide enough range so that the flow regimes encountered range from those in which a strong inlet vortex and a single trailing vortex were present, to those in which no inlet vortex existed, but two counter-rotating vortices trailed from the inlet.

3. At conditions where a strong vortex was present, measurements were made of the circulation around the inlet and the trailing vortices. It was found that their circulations were approximately equal and opposite, as had been previously hypothesized.

4. Velocity measurements and flow visualization showed that there was a second region of substantial axial vorticity inside the inlet, in addition to that associated with the inlet vortex. This was located at roughly the 'two o'clock' position, looking into the inlet.

5. The (axial) vortex filaments in this second vortical region are a continuation of the vortex lines associated with the trailing vortex. Some of these vortex lines thread through the boundary layers on the outside rear of the inlet; these are associated with the axial variation in circulation round the inlet. Other vortex lines, however, appear to come directly into the inlet from the core of the trailing vortex.

6. In contrast to many situations in which trailing vortices exist, because of the strong sink effect of the inlet, the flow in the core of the trailing vortex near the inlet is towards the inlet. The trace of the trailing vortex on the inlet, as indicated by the limiting streamlines, is thus a focus of attachment, rather than of separation.

7. As with the inlet vortex, the mechanism responsible for maintaining the trailing vortex is the production of vorticity in the core by vortex stretching. This, again, is in contrast to the usual trailing-vortex flow in which the vorticity is fed into the core from boundary layers on an upstream body.

8. Flow-visualization studies were also made of the transition between the inlet-vortex/trailing-vortex configuration and that of two trailing counter-rotating vortices. It was found that this transition is not gradual (as a function of CR, say) but occurs abruptly at a critical value of this parameter. In this transition, the lower trailing vortex moves downward to become the inlet vortex.

9. A limited parametric study was carried out to quantitatively define the changes in vortex strength and position as H/D and capture ratio are varied. Increasing H/D has a qualitatively, but not quantitatively, similar effect to decreasing CR.

The authors would like to thank Professor F. E. Marble for many insightful discussions on various aspects of this problem. They are also pleased to acknowledge the useful comments and recommendations of Professors E. E. Covert and J. L. Kerrebrock, and Messrs J. P. Nikkanen and D. L. Motycka, and the help rendered by F. H. Durgin and P. Lorber in coping with the Wright Brothers Wind Tunnel and Ms D. Park in coping with the authors during the manuscript preparation.

This research was supported by the Air Force Office of Scientific Research under contract No. F49620-82-K-0002, Dr J. D. Wilson, Program Manager.

REFERENCES

Boles, M. A. & Stockman, N. O. 1977 Use of experimental separation limits in the theoretical design of V/STOL inlets *AIAA Paper No.* 77–878.

De Siervi, F., Viguier, H. C., Greitzer, E. M. & Tan, C. S. Mechanisms of inlet vortex formation. *J. Fluid Mech.* **124**, 173–207.

Lighthill, M. J. 1963 Attachment and separation in three-dimensional flow. In *Laminar Boundary Layers* (ed. L. Rosenhead), pp. 72–82. Oxford University Press.

Liu, W., Greitzer, E. M. & Tan, C. S. 1985 Surface static pressures in an inlet vortex flow field. *Trans. ASME* J: *J. Engng Gas Turbines & Power* **107**, 387–393.

Maskell, E. C. 1955 Flow separation in three dimensions. *RAE Report* 2565.

Motycka, D. L. 1976 Ground vortex-limit to engine reverser operation. *Trans. ASME* J: *J. Engng Gas Turbines & Power* **98**, 258–266.

Perry, A. E. & Tan, D. K. M. 1984 Simple three-dimensional vortex motions in coflowing jets and wakes. *J. Fluid Mech.* **141**, 197–231.

SCHMIDT, D. P. & OKIISHI, T. H. 1977 Multistage axial-flow turbomachine wake production, transport and interaction. *AIAA J.* **15** (8), 1138–1145.

SHIN, H. W. & SHIPPEE, C. 1984 Quantitative investigation of inlet vortex flow field. *MIT Gas Turbine Laboratory Report No.* 179.

STOCKMAN, N. O. & FARRELL, C. A. 1977 Improved computer programs for calculating potential flow in propulsion system inlets. *NASA TM*-73728.

TOBAK, M. & PEAKE, D. J. 1982 Topology of three-dimensional separated flows. *Ann. Rev. Fluid Mech.* **14**.

YOUNGHANS, J. L. & PAUL, D. L. 1978 Considerations in inlet engine integration. In *The Aerothermodynamics of Aircraft Gas Turbine Engines* (ed. G. C. Oates), *AFAPL-TR*-78-52, Air Force Aero Propulsion Laboratory.